Journal of Colloid and Interface Science 386 (2012) 307–314

Contents lists available at SciVerse ScienceDirect

Journal of Colloid and Interface Science

www.elsevier.com/locate/jcis

Amino modified mesostructured silica nanoparticles for efficient adsorption of methylene blue

A.H. Karim [a], A.A. Jalil [b,*], S. Triwahyono [a], S.M. Sidik [a], N.H.N. Kamarudin [b], R. Jusoh [b], N.W.C. Jusoh [b], B.H. Hameed [c]

[a] Ibnu Sina Institute for Fundamental Science Studies, Faculty of Science, Universiti Teknologi Malaysia, 81310 UTM Johor Bahru, Johor, Malaysia
[b] Institute of Hydrogen Economy, Faculty of Chemical Engineering, Universiti Teknologi Malaysia, 81310 UTM Johor Bahru, Johor, Malaysia
[c] School of Chemical Engineering, Engineering Campus, Universiti Sains Malaysia, 14300 Nibong Tebal, Penang, Malaysia

ARTICLE INFO

Article history:
Received 1 May 2012
Accepted 12 July 2012
Available online 25 July 2012

Keywords:
Mesostructured silica nanoparticles
Adsorption
Methylene blue
Isotherm
Kinetic

ABSTRACT

In this work, mesostructured silica nanoparticles (MSN_{AP}) with high adsorptivity were prepared by a modification with 3-aminopropyl triethoxysilane (APTES) as a pore expander. The performance of the MSN_{AP} was tested by the adsorption of MB in a batch system under varying pH (2–11), adsorbent dosage (0.1–0.5 g L^{-1}), and initial MB concentration (5–60 mg L^{-1}). The best conditions were achieved at pH 7 when using 0.1 g L^{-1} MSN_{AP} and 60 mg L^{-1}MB to give a maximum monolayer adsorption capacity of 500.1 mg g^{-1} at 303 K. The equilibrium data were evaluated using the Langmuir, Freundlich, Temkin, and Harkins–Jura isotherms and fit well to the Freundlich isotherm model. The adsorption kinetics was best described by the pseudo-second order model. The results indicate the potential for a new use of mesostructured materials as an effective adsorbent for MB.

1. Introduction

The disposal of untreated effluents from many dye industries to the surrounding environment often leads problems for aquatic life and humans. Therefore, it is mandatory to treat these dye wastewaters prior to discharge into the receiving body of water. Among various physical treatment methods, adsorption using activated carbon is the most widely used technique in industries for the removal of dyes, but this method has been found to be ineffectual due to its high cost and reusability [1].

Recently, microporous inorganic adsorbents (e.g., zeolites) and mesoporous silica (e.g., MCM-41 and SBA-15) with unique surface and pore properties as well as high surface areas have been extensively investigated as alternatives to carbon adsorbents for the liquid adsorption of dissolved pollutants in water [2,3]. They have also been verified as economical and useful high-capacity adsorbents because they can be regenerated after multiple uses [4]. However, these classes of mesostructured materials possess some shortcomings and need to be extended to wider classes of mesostructured silica materials. In response to this, mesostructured silica nanoparticles (MSN) have become increasingly important because of their high surface area (>1000 m^2 g^{-1}), thermal and mechanical stability, highly uniform pore distribution, tunable pore size, and unique hosting properties [2–7]. These remarkable features mean that MSN are exploited in a wide range of applications, including catalyst supports [5], separation agents [6], carriers for drug delivery [7], and as effective adsorbents [2,8,9]. However, to some extent, their applications, particularly in adsorption, are still limited due to a lack of control in terms of particle and/or pore size. To this purpose, surface functionalization by organic groups on mesostructured materials has been employed using two general methods, namely post-grafting and co-condensation synthesis [10]. Of these two methods, the latter allows for better control of the loading and distribution of organic groups [11].

Therefore, herein, we report on a facile preparation method for MSN using an amine, namely APTES (3-aminopropyl triethoxysilane) as a pore expander, which produced a mesostructured material (MSN_{AP}) with high specific surface area. The synthesized MSN was characterized by analytical techniques such as X-ray diffraction patterns, Fourier transform infrared spectroscopy, nitrogen physisorption, scanning electron microscopy, and transmission electron microscopy. The adsorption capability of MSN_{AP} was studied and compared with unmodified mesostructured silica nanoparticles (MSN_{UN}) in the adsorption of methylene blue (MB). The adsorption equilibrium and kinetics of the adsorption were also investigated.

2. Materials and methods

2.1. Materials

Cetyltrimethylammonium bromide (CTAB), ethylene glycol (EG), tetraethyl orthosilicate (TEOS), methylene blue (MB), and

* Corresponding author. Fax: +60 7 5536165.
E-mail address: aishah@cheme.utm.my (A.A. Jalil).

0021-9797/$ - see front matter © 2012 Elsevier Inc. All rights reserved.
http://dx.doi.org/10.1016/j.jcis.2012.07.043

Nomenclature

C_0	initial MB concentration (mg L^{-1})	k_2	pseudo-second order rate constant (mg g^{-1} min^{-1})
C_t	MB concentration at time t of reaction (mg L^{-1})	k_{id}	constant of intraparticle diffusion (mg g^{-1} $min^{-1/2}$)
C_e	MB concentration at equilibrium time (mg L^{-1})	C	thickness of the boundary layer
V	volume of the MB solution (L)	K_L	langmuir constant (L mg^{-1})
M	mass of MSN (g)	K_F	Freundlich adsorbent capacity
c	BET constant	K_T	Temkin constant (L mg^{-1})
P	equilibrium pressure	n_F	heterogenity factor
P_o	saturation pressure	q_{max}	maximum adsorption capacity (mg g^{-1})
v	adsorbed gas quantity	R	gas constant (8.314 J mol^{-1} K^{-1})
v_m	monolayer adsorbed gas quantity	T	absolute temperature (K)
q_e	adsorption uptake at equilibrium conditions (mg g^{-1})	A_{HJ}	Harkins–Jura constant
q_t	adsorption uptake at time t (mg g^{-1})	B_{HJ}	Harkins–Jura constant
k_1	pseudo-first order rate constant (min^{-1})		

3-aminopropyl triethoxysilane (APTES) were purchased from Merck Sdn. Bhd., Malaysia. Ammonium hydroxide solution (NH_4OH) was obtained from QRec, Malaysia. All of the chemicals were used as received without further treatment.

2.2. Synthesis of mesostructured materials

Modified mesostructured silica nanoparticles (MSN_{AP}) were prepared by co-condensation and the sol–gel method. The CTAB surfactant, EG, and NH_4OH solution were dissolved in 700 mL of water with the following mole composition, respectively: 0.0032:0.2:0.2:0.1. After vigorous stirring for about 30 min with heating, 1.2 mmol TEOS and 1 mmol APTES were added to the clear mixture to give a white suspension solution. This solution was then stirred for another 2 h, and the samples were collected by centrifugation. The synthesized MSN were dried at 333 K and calcined at 823 K for 3 h to remove the surfactant. Untreated MSN (MSN_{UN}) was prepared by similar procedure but excluding the APTES addition during the process.

2.3. Characterization of MSN

The crystalline structure of samples was determined by X-ray diffraction (XRD) recorded on a Bruker AXS D8 X-ray powder diffractometer (Cu Kα radiation, λ = 1.5418 Å). Transmission electron microscopy (TEM) was carried out using a JEOL JEM-2100F microscope. The samples were ultrasonically dispersed in acetone and deposited on an amorphous, porous carbon grid. Field-emission scanning electron microscopy (using a JEOL JSM-6701F microscope) was conducted to observe the topology of the samples. Nitrogen physisorption was measured at 77 K using a Quantachrome Autosorb-1 analyzer. Prior to measurements, the samples were evacuated for 24 h at 573 K. Specific surface area (S_{BET}) values were calculated from the BET isotherm plots [12], while the total pore volume and pore size distributions were calculated using the Barrett, Joyner, and Halenda (BJH) method [13] from the desorption isotherm. FT-IR spectroscopy (using a Perkin Elmer Spectrum GX FTIR spectrometer) was performed to identify the chemical functional groups present in the samples. The substance was finely ground and dispersed into KBr powder-pressed pellets using a ratio of approximately 1 mg sample/200 mg KBr. IR absorbance data were obtained over a range of wavenumbers from 4000–400 cm^{-1}.

2.4. Adsorption study

The activity of the adsorbents was tested for the adsorption of MB. This was performed in batches consisting of MB solution at various concentrations (5–60 mg L^{-1}). The solution was stirred at room temperature and 300 rpm to uniformly disperse the adsorbent with a dosage 0.1 g L^{-1}. The desired pH of the dye solution was achieved via adjustment with 0.1 M HCl or 0.1 M NaOH. During the process, aliquots of 2 ml were withdrawn at pre-determined time intervals and centrifuged in a Hettich Zentrifugen Micro 120 before being analyzed by UV–Vis spectrophotometer (Agilent Technologies) to determine the residual concentration of MB. Each set of experiments was performed three times. The adsorption band of MB was taken at a maximum wavelength (λ_{max}) of 664 nm and the adsorption uptake, q_t (mg g^{-1}), of the adsorbent was calculated using the following equation:

$$q_t = \frac{(C_o - C_t)V}{m} \quad (1)$$

where C_o and C_t (mg L^{-1}) are the concentrations of MB at the initial time and at time t, respectively, V (L) is the volume of the solution and m (g) is the mass of the adsorbent used.

For the kinetics studies, the adsorbent (at a dosage of 0.1 g L^{-1}) was placed in contact with the eight different initial concentrations of MB solution. The agitation speed was kept constant (500 rpm), and analyses of the solutions were carried out using the same procedure as in the adsorption study.

3. Results and discussion

3.1. Characteristics of the adsorbent material

Fig. 1 shows the low-angle powder XRD patterns of the synthesized mesostructured silica in the range of 2θ = 1.5–10°. Distinct diffraction peaks were observed at 2θ = 2.35°, 4.10°, and 4.75°, which were indexed as (100), (110), and (200) reflections, respectively. This typical mesostructured silica with hexagonal *p6mm* structure peaks formed by the 2D hexagonal array of mesostructure is in agreement with the reported pattern [14]. Furthermore, the relatively high intensity of the (100) peak in MSN_{AP} as compared to MSN_{UN} illustrates that the former was produced with a more highly ordered arrangement of the channels [15]. The shift of the two-theta position in the (100) peak of MSN_{AP} indicates the possible shrinkage of channels and a more ordered arrangement of the structure [15].

The nitrogen adsorption–desorption isotherms are given in Fig. 2A, exhibiting an H1 hysteresis loop with a type IV isotherm, which is the typical adsorption profile for mesostructure [16]. Three well-defined stages of the isotherm shape were identified as follows: (1) a gradual increase in nitrogen uptake at a low relative pressure, corresponding to monolayer/multilayer adsorption on pore walls, (2) a step at an intermediate relative pressure, indi-

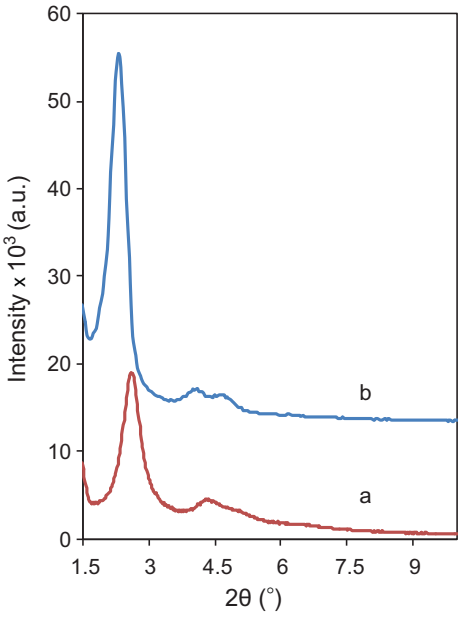

Fig. 1. XRD pattern of MSN_{UN} (a) and MSN_{AP} (b).

cating capillary condensation within the mesopores, and (3) a plateau with a slight inclination at high relative pressures associated with multilayer adsorption on the external surface of the samples [17]. A steep increase in the isotherms at a relative pressure between 0.25 and 0.35 explains N_2 filling of rather uniform mesopores by capillary condensation [18]. Besides, MSN_{AP} shows a much steeper climb than MSN_{UN} near the limit of saturated pressure (at intermediate relative pressure), suggesting that capillary condensation within its mesopore is relatively higher. The difference might come from the porous structure of MSN_{AP}, which is believed to be much ordered and larger in size [17].

Fig. 2B depicts the pore size distribution of MSN_{AP} by the BJH analysis of nitrogen adsorption. The presence of a narrow peak in the mesoporous range shows that mesopore channels are present in MSN_{AP}. Furthermore, the narrow peak demonstrates the occurrence of smaller mesostructures with a uniform distribution [17]. In Fig. 2B, the MSN_{AP} plot (b) shows the presence of a relatively higher number of pores with larger diameters compared to MSN_{UN}, which most probably responsible to the efficient adsorption of MB.

Table 1
Textural properties of MSNs.

Sample	Surface area, S_{BET} ($m^2\ g^{-1}$)	Average pore size (nm)	Pore volume, V_{pore} ($cm^3\ g^{-1}$)
MSN_{UN}	1242	3.56	1.06
MSN_{AP}	1277	3.64	1.16

The degree of interaction between adsorbent and adsorbate could be also represented by a *c* constant calculated from the following BET equation,

$$\frac{1}{v[(P_o/P)-1]} = \frac{c-1}{v_m c}\left(\frac{P}{P_o}\right) + \frac{1}{v_m c} \quad (2)$$

This constant depends on the fraction of surface uncovered by adsorbate when sufficient adsorption occurred in monolayer and it varies from solid to solid. In this study, the *c* values obtained from BET analysis for MSN_{AP} and MSN_{UN} were 82.99 and 60.48, respectively, which categorized as relatively high values. The low *c* values represent weak gas adsorption due to low surface area of the solids [17,19,20].

A summary of the corresponding textural properties of MSN_{UN} and MSN_{AP} is provided in Table 1. It can be seen that MSN_{AP} showed a larger BET surface area, pore size, and pore volume as compared to MSN_{UN}. These differences could be due to the synthesis method of the two MSN samples. APTES is believed to function as a pore expander [21] and stabilizer of the mesostructure.

The surface structure and morphology of MSN_{AP} was investigated using FESEM and TEM. Fig. 3A shows MSN_{AP} as fairly uniform spherical particles with an average size of 70–150 nm. Its mesostructure was further confirmed by TEM analysis. The TEM image (Fig. 3B) clearly shows well-ordered pores and indicates that a 2-D hexagonal *p6mm* mesostructure is present [22]. These results are in accordance with those measured from the low-angle XRD patterns and N_2 adsorption–desorption analysis.

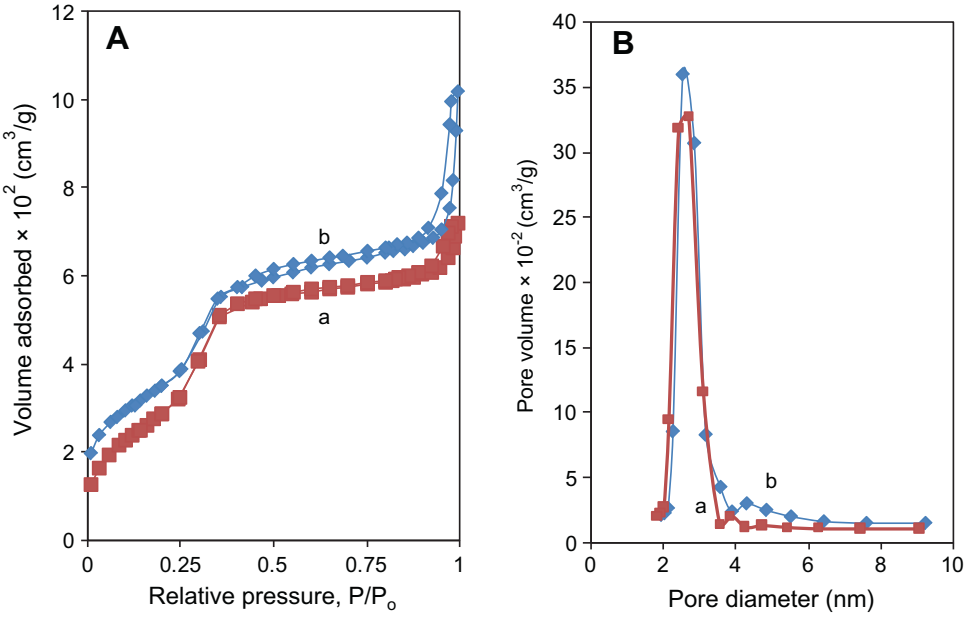

Fig. 2. (A) Nitrogen adsorption–desorption isotherms of MSN_{UN} (a) and MSN_{AP} (b). (B) Pore distribution of MSN_{UN} (a) and MSN_{AP} (b).

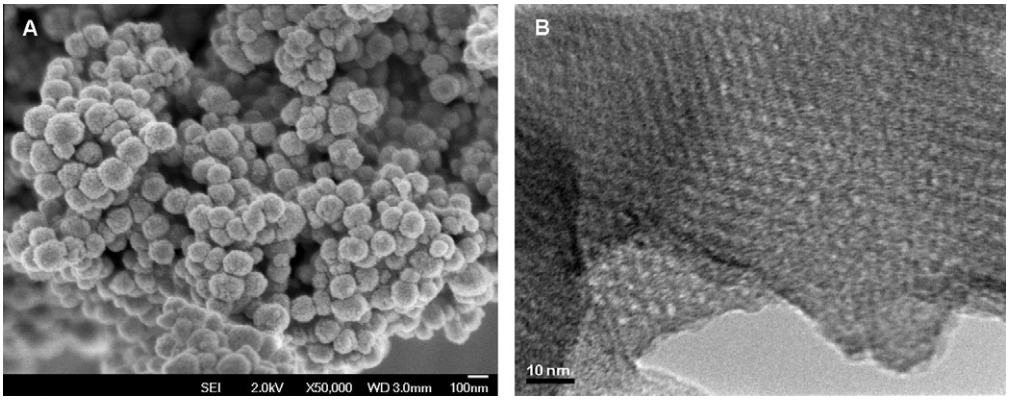

Fig. 3. (A) FESEM and (B) TEM images of mesostructured silica nanoparticles.

FT-IR measurements were performed to identify the structural differences between the MSN samples and to demonstrate the presence of MB adsorbed on the surface of MSN. Fig. 4 illustrates the FT-IR spectra of MSN_{UN} and MSN_{AP} before and after the adsorption of MB. The MSN samples exhibited IR peaks at the bands attributed to Si—O—Si bending (472 cm^{-1}), defective structures (601 cm^{-1}), Si—O—Si symmetric stretching (811 cm^{-1}), external Si—OH groups (978 cm^{-1}), Si—O—Si asymmetric stretching (1106 cm^{-1}), water molecules retained by siliceous materials (1652 cm^{-1}), and —OH stretching (3480 cm^{-1}, broad) [23,24]. After modification with APTES, the MSN still retained its siliceous structure, which confirmed that no major changes had occurred in the formation of its framework. After MB adsorption, the relative intensity of all Si—O vibration modes at 478 cm^{-1}, 976 cm^{-1}, and 1104 cm^{-1} became more intense, suggesting the existence of stronger Si—O—Si interactions in the presence of foreign molecules in the synthesis step. The increase in intensity in the range of 1130–1000 cm^{-1} clearly indicates that most of the Si—O bonds on the inner surface of MSN were involved in the adsorption process.

New bands at 1500 cm^{-1}, 1406 cm^{-1}, and 1335 cm^{-1} appeared after the adsorption process, corresponding to C=C aromatic and C—N aromatic bonds, respectively. These new bands were associated with the aqueous solution of MB, demonstrating that MB was successfully loaded onto the surface of MSN. The increase in the band 1652 cm^{-1} might be associated with the aqueous solution of MB, while the appearance of the band 1639 cm^{-1} was attributed to the overlay of the N—H group from MB [25,26].

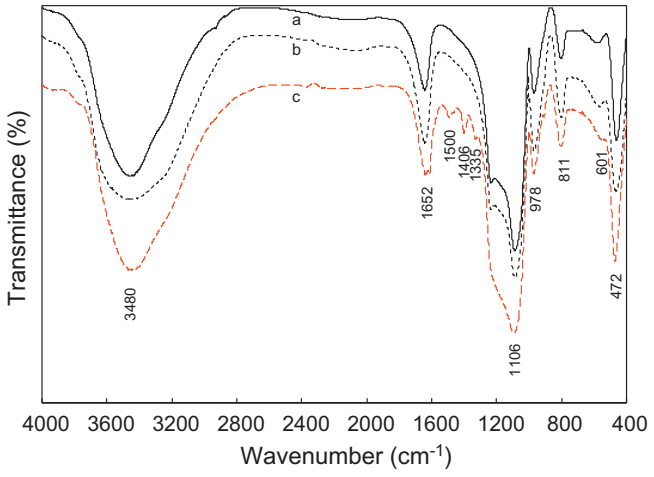

Fig. 4. FTIR Spectra of MSN_{UN} (a), MSN_{AP} (b), and MSN_{AP}-MB (c).

3.2. Adsorption studies

3.2.1. Performance of mesostructured silica and effect of initial concentration

The performance of the synthesized adsorbents is illustrated in Fig. 5. It clearly observed that MSN_{AP} (true line) shows significantly good adsorptivity compared to MSN_{UN} (dotted line) toward 60 mg L^{-1} of MB. The adsorption uptake of MB by MSN_{AP} increased rapidly in the first 10 min and then gradually increased until the equilibrium was achieved at 20 min to give 165 mg g^{-1} of equilibrium uptake. The equilibrium uptake achieved by the MSN_{UN} was 113 mg g^{-1}. The short contact time required to reach equilibrium as well as the higher adsorption uptake demonstrates the effectiveness of the APTES modified adsorbent.

The effect of initial concentration of MB on the adsorption of MSN_{AP} is also shown in Fig. 5, with eight different concentrations ranging from 5 to 60 mg L^{-1}. An increase in initial dye concentration leads to an increase in the adsorption uptake of MB on MSN_{AP}. This is due to an increase in the driving force of the concentration gradient, as an increase in the initial dye concentration [27].

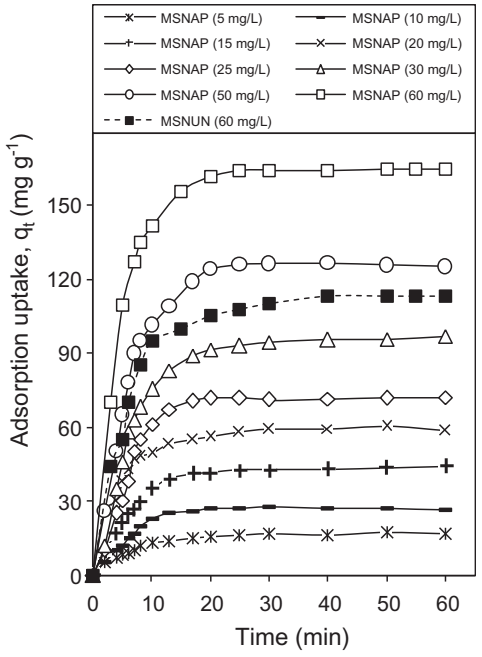

Fig. 5. Performance of MSN_{UN} (solid symbols) and MSN_{AP} (open symbols) toward adsorption of MB (adsorbent dosage 0.1 g L^{-1}, initial pH 7, 303 K).

3.2.2. Effect of pH

Fig. 6 shows the effect of pH in the range of 2–11 on the adsorption of MB onto MSN_{AP}. It could be observed that the adsorption uptake at equilibrium was increased with increasing pH, and a maximum adsorption uptake at equilibrium of 66 mg g^{-1} was achieved at pH 7. This can be explained by the electrostatic interactions between cationic MB and the negatively charged MSN_{AP} surface. At lower pH, the competition between cationic MB and excess H^+ ions obstructed the adsorption process, but a decrease in the proton concentration with increasing pH favored the reaction [28]. The adsorption uptake at equilibrium slightly decreased at higher pH, possibly due to the competition between OH^- ions and negatively charged MSN_{AP} ions in the system [29].

3.2.3. Effect of adsorbent dosage

The amount of surface available for adsorption certainly depends on the mass of the adsorbent. For this reason, the effect of MSN_{AP} dosage on MB adsorption was studied in the range of 0.1–0.5 g L^{-1}, at the optimum pH 7 and initial concentration of 10 mg L^{-1} of MB (Fig. 7). It was clearly observed that the adsorption uptake at equilibrium of MB increased with decreasing adsorbent dosage, in which the highest adsorption uptake at equilibrium of 85 mg g^{-1} was attained when the dosage of MSN_{AP} was 0.1 g L^{-1}. The achievement of high adsorption uptake with a relatively low MSN_{AP} dosage indicates the high affinity of the adsorbent for MB adsorption in the system. A lower adsorbent dosage means that a smaller overall total surface area of MSN_{AP} is exposed, and hence, more MB anions were adsorbed onto the surface per gram unit of MSN_{AP}, which led to the higher adsorption uptake [30].

3.2.4. Equilibrium isotherms studies

The analysis of the equilibrium adsorption isotherm model is a prerequisite for predicting the adsorption uptake of the adsorbent, which is one of the main parameters required for designing an optimized adsorption system. Four available isotherm models, that is, the Langmuir [31], Freundlich [32], Temkin [33], and Harkins–Jura [34] models, are used for this purpose. The linear forms of these four isotherm models were simplified and represented as follows:

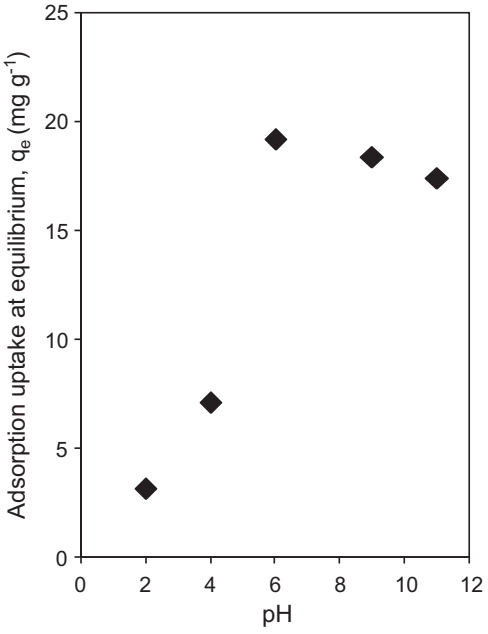

Fig. 6. Effect of pH on adsorption of MB on MSN_{AP} (adsorbent dosage 0.1 g L^{-1}, initial MB concentration 10 mg L^{-1}, 303 K).

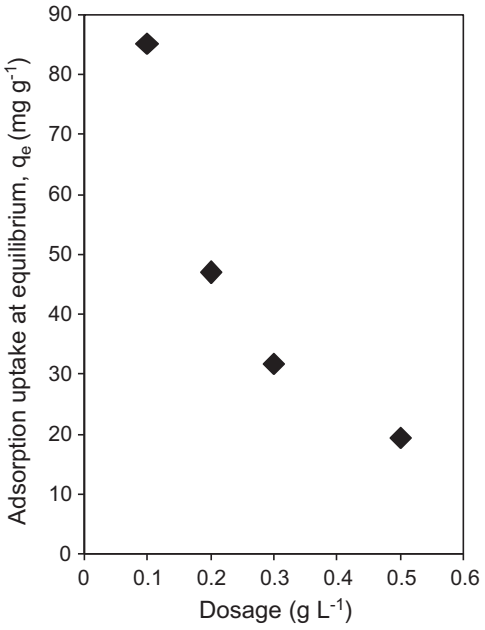

Fig. 7. Effect of MSN_{AP} dosage (initial MB concentration 10 mg L^{-1}, initial pH 7, 303 K).

$$\text{Langmuir}: \quad \frac{1}{q_e} = \frac{1}{q_{\max} K_L C_e} + \frac{1}{q_{\max}} \tag{3}$$

$$\text{Freundlich}: \quad \log q_e = \log K_F + \frac{1}{n_F} \log C_e \tag{4}$$

$$\text{Temkin}: \quad q_e = \frac{RT}{b_T} \ln K_t + \frac{BT}{b_T} \ln C_e \tag{5}$$

$$\text{Harkins} - \text{Jura}: \quad \frac{1}{q_e} = \frac{B_{HJ}}{A_{HJ}} + \frac{\log C_e}{A_{HJ}} \tag{6}$$

Fig. 8 shows the plotted models including the fitted models; the extracted isotherm information is summarized in Table 2. Referring to Fig. 8 as well as to Table 2, it was clear that both Langmuir and Freundlich models provided a good fit for the experimental equilibrium adsorption data. The Langmuir model assumes a complete monolayer of adsorption, in which there is no transmigration of the adsorbate on the surface plane [31]. This system involves a homogeneous surface with equal energy and equally available sites for adsorption [35]. The Langmuir $q_{\max}$ value was 500.1 mg g^{-1}, and K_L constant is 0.0085. The R_L value [$R_L = 1/(1 + K_L C_0)$] for the system, which demonstrates the favorability of the adsorption, was calculated to be 0.662, indicating the favorable adsorption of MB occurred because the value falls between 0 and 1 [36].

However, the higher accuracy ($R^2 = 0.999$) revealed that the Freundlich isotherm model better described the adsorption of MB onto MSN_{AP}. The Freundlich model [32] illustrates the adsorption of MB by pinpointing heterogeneously distributed adsorption sites on MSN_{AP}. The value of n_F, which is known as heterogeneity factor, was used to identify the adsorption whether it is linear ($n_F = 1$), chemical process ($n_F < 1$), and physical process ($n_F > 1$). Hence, in this study, linear adsorption process is favorable with the n_F value 1, while the K_F value, which is an indicator of adsorption capacity, indicated a high MB adsorptive capacity of MSN_{AP} from aqueous solution studied [37]. Besides, the inconsistent arrangement of the heterogeneously adsorbed MB has been shown to promote the development of local multilayers [34]. A similar phenomenon

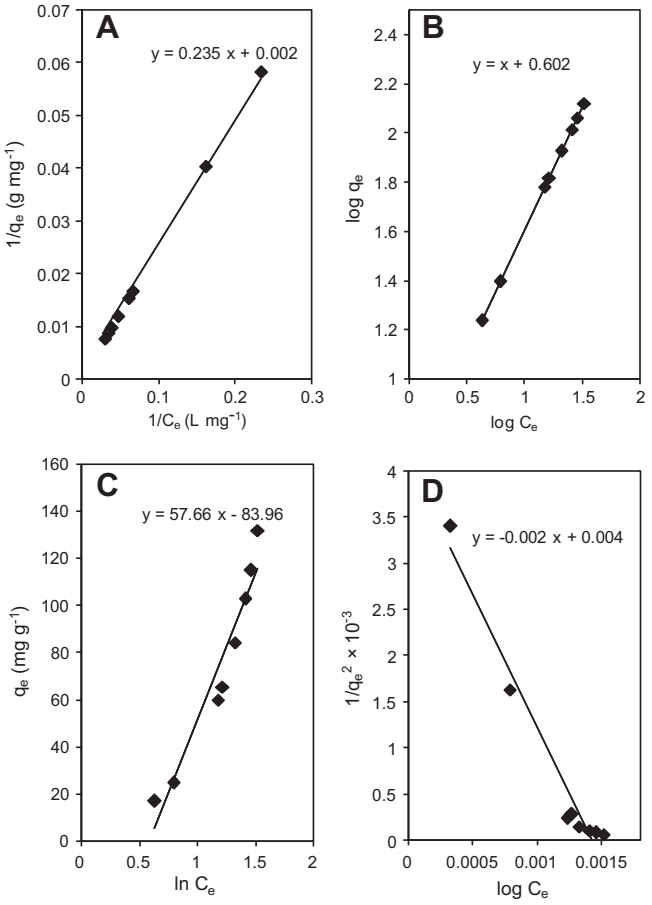

Fig. 8. Linear plots of isotherm models for adsorption of MB onto MSN_{AP} (adsorbent dosage 0.1 g L^{-1}, initial pH 7, 303 K): (A) Langmuir, (B) Freundlich, (C) Temkin, and (D) Harkins–Jura.

Table 2
Fitted isotherm models for MB adsorption onto MSN_{AP}.

Isotherm	Parameters	Values
Langmuir	q_{max} (mg g^{-1})	500.1
	K_L (L mg^{-1})	0.0085
	R_L	0.662
	R^2	0.994
Freundlich	K_F (m/g) (l/mg)$^{1/n}$	3.33
	n_F	1.00
	R^2	0.999
Temkin	b	43.6
	K_T (L g^{-1})	0.23
	R^2	0.943
Harkins–Jura	A_{HJ}	500
	B_{HJ}	2
	R^2	0.961

was observed in the adsorption of cationic dyes onto other mesostructured silica materials [22].

Table 2 further shows that the experimental adsorption data also had an adequate correlation with the Temkin isotherm. Like the Freundlich model, the Temkin model considers interactions with the adsorbate, assuming that the adsorption heat of all molecules decreases linearly when the layer is covered and that the adsorption has a maximum energy distribution of uniform bonds [35]. K_T is Temkin equation parameter adequate with boundary constant adequate with maximum of boundary energy. The positive value of the constant B_T ($B_T = RT/b$) indicates an exothermic process since b is related to the heat of adsorption. Also, the B_T value of 57.7 kJ mol^{-1} illustrates that the bonds between MB ions and the MSN_{AP} surface are very strong. Besides, as shown in Table 2, the experimental adsorption data fitting with the Harkins–Jura model confirms the occurrence of multilayer adsorption due to the heterogeneous pore distribution [35]. Therefore, this model further demonstrates that MSN_{AP} is mesostructure [38], in agreement with the TEM results.

3.2.5. Kinetics studies

Adsorption kinetics is essential for understanding the adsorbate uptake rate and the mechanism of the process. In order to evaluate the adsorption behavior of MB onto MSN_{AP}, the experimental data from this study were fitted to three conventional kinetic models, including the Lagergren pseudo-first order [39], the Ho pseudo-second order [40], and the Weber–Morris intraparticle diffusion models [41]. The linear forms of these models are given as:

$$\text{Pseudo-first order equation}: \quad \ln(q_e - q_t) = \ln q_e - k_1 t \tag{7}$$

$$\text{Pseudo-second order equation}: \quad \frac{t}{q_t} = \frac{1}{k_2 q_e^2} + \frac{t}{q_e} \tag{8}$$

$$\text{Weber—Morris equation}: \quad q_t = k_{id} t^{1/2} + C \tag{9}$$

The summary of the models used at three different temperatures and the kinetic information obtained from the pseudo-first and pseudo-second order plots are presented in Table 3. Due to the closer value of adsorption uptake at equilibrium (q_e) calculated from the pseudo-second order model with the experimental value compared to the pseudo-first order model, it could be concluded that the pseudo-second order kinetic model was the best fit for the experimental data, as shown in Fig. 9. Similar kinetic behavior was also observed for the adsorption of MB onto SBA-3 [28], AlMCM-41 [42], and SBA-15 [22]. Additionally, Table 3 reveals that as the temperature increased, the adsorption uptake decreased, leading to the conclusion that the adsorption of MB onto MSN_{AP} is an exothermic process.

To identify the step possibly controlling the adsorption of MB onto MSN_{AP} under the selected conditions, the experimental data were then fitted to the Weber–Morris equation, which is the most commonly tested model. It can be seen in Fig. 10 that the plot of

Table 3
Coefficient of pseudo-first and -second order adsorption kinetic models.

Initial conc. (mg L^{-1})	$q_{e,exp}$ (mg g^{-1})	Pseudo-first order			Pseudo-second order		
		q_e (mg g^{-1})	k_1 (min^{-1})	R^2	q_e (mg g^{-1})	k_2 (10^{-2} g mg^{-1} min^{-1})	R^2
5	17.2	3.30	0.053	0.988	22.2	0.567	0.982
10	26.8	3.12	0.045	0.972	37.0	0.261	0.977
15	43.6	5.47	0.073	0.989	66.7	0.144	0.970
20	60.2	4.84	0.052	0.952	66.7	0.229	0.991
25	71.7	10.2	0.15	0.912	125	0.073	0.901
30	95.8	7.42	0.069	0.995	167	0.051	0.929
50	126	9.73	0.01	0.954	200	0.050	0.944
60	164	6.43	0.045	0.977	370	0.048	0.996

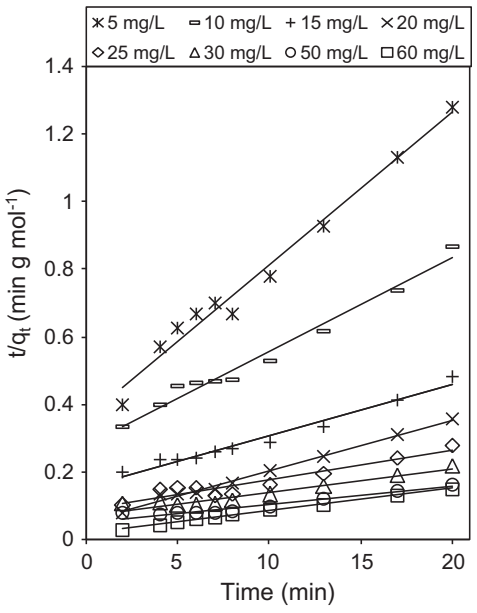

Fig. 9. Pseudo-second order kinetics model for adsorption of MB onto MSN_{AP} (adsorbent dosage 0.1 g L^{-1}, initial pH 7, 303 K).

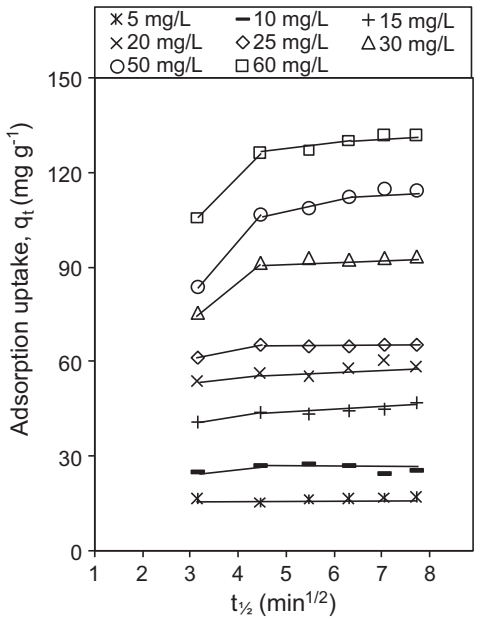

Fig. 10. Intraparticle diffusion plot for adsorption of MB onto MSN_{AP}.

the amount of dye adsorbed (q_t) versus the square root of time ($t^{1/2}$) is not linear over the entire time range, but is instead separated into two steps at a lower initial concentration of 5–20 mg L^{-1} MB and into multiple steps at 30 mg L^{-1} MB and above. These results show that intraparticle diffusion is not the only rate-controlling step in this adsorption because the plot is not linear and does not pass through the origin [30,43]. The smaller number of MB molecules in the system at lower initial concentrations may have led to their rapid intraparticle diffusion and surface adsorption on the surface or pores of MSN_{AP}. However, collisions among the MB molecules at higher concentrations ($\geqslant$30 mg L^{-1}) may have caused the adsorption to take place through several consecutive steps: film diffusion, intraparticle diffusion, and adsorption onto the surface or pores of MSN_{AP} [44,45]. The final step seems to have achieved equilibrium because the adsorption sites were almost saturated [30].

3.3. Comparison of MSN with various mesostructured materials

Table 4 lists a comparison of the maximum adsorption capacities (q_{max}) of mesostructured silica adsorbents for MB. Although MCM-41 [46], MCM-48 [7], and MCM-50 [7] possess large surface area (>1000 m^2 g^{-1}), the adsorption uptake is lower than MSN. The Al, TiO_2, and $H_3PW_{12}O_{40}$—TiO_2 modified MCM-41 also shows lower adsorptivity toward MB [42,46]. The MSN had a relatively large adsorption uptake (500.1 mg g^{-1}), suggesting that it is a competent material for the adsorption of MB from aqueous solution. Another family of mesostructured materials, SBA, has also been widely used for dye removal. SBA-15 [47] and SBA-3 [28] have a higher adsorption uptake compared to MCM, most probably due to their richer pore channel structure and larger mean pore size [47]. However, the MSN_{AP} adsorbent prepared in this study has a greater maximum adsorption uptake than SBA, likely as a result of the larger pore volume. The relatively large adsorption uptake of MSN_{AP} proves its great adsorption capability.

4. Conclusion

This work illustrates the potential of amino modified MSN adsorbent to shorten the time of adsorption of MB from aqueous solution. The best conditions were achieved at pH 7, 0.1 g L^{-1}, and 60 mg L^{-1}, with a maximum adsorption capacity of 500.1 mg g^{-1} at 303 K. The equilibrium data fit well to the Freundlich adsorption isotherm, which reflects the multilayer adsorption of MB particles onto the synthesized mesostructured materials. The kinetics adsorption was a pseudo-second order process. The adsorption process was relatively faster, with equilibrium achieved within 20 min, compared to other type of mesoporous silicas such

Table 4
Comparison of maximum adsorption capacities of various mesoporous silica adsorbents for MB.

Adsorbent	Surface area (m^2 g^{-1})	Pore volume (cm^3 g^{-1})	Average pore size (nm)	Initial concentration, C_o (mg L^{-1})	Maximum adsorption capacity, q_e (mg g^{-1})	Refs.
MSN	1277	1.16	3.64	5–80	500.1	This study
MCM-41	1071	–	2.76	20–1000	54	[46]
AlMCM-41	–	–	–	0.319–3.19	66.5	[42]
TiO_2/MCM-41	590	0.21	–	30	54.4	[46]
TT-MCM-41	450	0.16	–	30	60.8	[46]
MCM -22	490	–	–	3.19–31.9	57.6	[3]
MCM-48	1647	1.56	3.8	3.19–31.9	10.6	[7]
MCM-50	1222	1.71	5.6	3.19–31.9	21.6	[7]
SBA-15	659	0.83	5.27	15.9–159	51.04	[22]
SBA-15	420	0.91	10.7	30–110	280	[47]
SBA-3	1423	0.93	–	50–150	285.7	[28]

as MCM and SBA, which achieved equilibrium time within 4 h (MCM-41), 60 min (SBA-15), and 70 min (SBA-3) [7,22,28]. Besides, the maximum adsorption capacity of the MSN_{AP} was relatively higher than several mesoporous silica adsorbents reported in the literature. With this remarkable performance, amino modified MSN suggests its application toward adsorption of various organic pollutants as well as to large-scale process.

Acknowledgments

The authors are grateful for the financial supports by the Research University Grant from Universiti Teknologi Malaysia (Grant No. 01H95) and the award of my PhD Scholarship (Ainul Hakimah Karim) from the Ministry of Higher Education Malaysia. We are also thankful to The Hitachi Scholarship Foundation and Dr. Rino Mukti for their support and advice.

References

[1] A. Mittal, J. Mittal, A. Malviya, D. Kaur, V.K. Gupta, J. Colloid Interface Sci. 342 (2010) 518.
[2] Q. Qin, J. Ma, K. Liu, J. Hazard. Mater. 162 (2009) 133.
[3] S. Wang, H. Li, L. Xu, J. Colloid Interface Sci. 295 (2006) 71.
[4] C.M. Maroneze, H.A. Magosso, A.V. Panteleimonov, Y.V. Kholin, Y.J. Gushikem, J. Colloid Interface Sci. 356 (2011) 248.
[5] D. Tang, L. Zhang, Y. Zhang, Z.-A. Qiao, Y. Liu, Q. Huo, J. Colloid Interface Sci. 369 (2012) 338.
[6] E. Vega, C. Marzabadi, Y. Kazakevich, A.Y. Fadeev, J. Colloid Interface Sci. 359 (2011) 542.
[7] S. Wang, Microporous Mesoporous Mater. 117 (2009) 1.
[8] N. Gargiulo, F. Pepe, D. Caputo, J. Colloid Interface Sci. 367 (2012) 348.
[9] J. Li, X. Miao, Y. Hao, J. Zhao, X. Sun, L. Wang, J. Colloid Interface Sci. 318 (2008) 309.
[10] K.K. Sharma, T. Asefa, Angew. Chem. Int. Ed. 46 (2007) 2879.
[11] G. Wang, A.N. Otuonye, E.A. Blair, K. Denton, Z. Tao, T. Asefa, J. Solid State Chem. 182 (2009) 1649.
[12] S. Brunauer, P.H. Emmett, E. Teller, J. Am. Chem. Soc. 60 (1938) 309.
[13] E.P. Barrett, L.G. Joyner, P.P. Halenda, J. Am. Chem. Soc. 73 (1951) 373.
[14] D.Y. Zhao, J.L. Feng, Q.S. Huo, N. Melosh, G.H. Fredrickson, B.F. Chmekka, G.D. Stucky, Science 279 (1998) 548.
[15] S.A. El-Safty, A. Shahat, M. Rabiul Awual, J. Colloid Interface Sci. 359 (2011) 9.
[16] C.T. Kresge, M.E. Leonowicz, W.J. Roth, J.C. Vartuli, J.S. Beck, Nature 359 (1992) 710.
[17] S.J. Gregg, K.S.W. Sing, Adsorption Surface Area and Porosity, first ed., Academic Press, London, 1967.
[18] K.S.W. Sing, D.H. Everett, R.A.W. Haul, L. Moscou, R.A. Pierotti, J. Rouquerol, T. Siemieniewska, Pure Appl. Chem. 57 (1985) 603.
[19] S. Lowell, J. Shields, G. Charalambous, J. Manzione, J. Colloid Interface Sci. 86 (1982) 191.
[20] F. Salvador, C. Sánchez-Jiménez, M.J. Sánchez-Montero, A. Salvador, Stud. Surf. Sci. Catal. 144 (2002) 379.
[21] H. Yang, Q. Feng, J. Hazard. Mater. 180 (2010) 106.
[22] C.-H. Huang, K.-P. Chang, H.-D. Ou, Y.-C. Chiang, C.-F. Wang, Microporous Mesoporous Mater. 141 (2011) 102.
[23] A.M. Klonkowski, T. Widernik, B. Grobelna, W.K. Jozwiak, H. Proga, E. Szubiakiewicz, J. Sol-Gel Sci. Technol. 20 (2000) 161.
[24] L.P. Singh, S.K. Agarwal, S.K. Bhattacharyya, U. Sharma, S. Ahalawat, Nanomater. Nanotechnol. 1 (2011) 44.
[25] E.M. Flanigen, H. Khatami, H.A. Szymanski, Adv. Chem. Ser. 101 (1971) 201.
[26] J. Klinowski, in: J. Klinowski, P.J. Barrie (Eds.), Recent Advances in Zeolite Science, Proceedings of the 1989 Meeting of the British Zeolite Association, Cambridge.
[27] D.J. Ju, I.G. Byun, C.H. Lee, G.H. An, T.J. Park, Water Pract. Technol. 1 (2006) 3.
[28] M. Anbia, S.A. Hariri, Desalination 261 (2010) 61.
[29] I. Moriguchi, M. Honda, T. Ohkubo, Y. Mawatari, Y. Teraoka, Catal. Today 90 (2004) 297.
[30] A.A. Jalil, S. Triwahyono, S.H. Adam, N.D. Rahim, M.A.A. Aziz, N.H.H. Hairom, N.A.M. Razali, M.A.Z. Abidin, M.K.A. Mohamadi, J. Hazard. Mater. 181 (2010) 755.
[31] I.J. Langmuir, Am. Chem. Soc. 39 (1917) 1848.
[32] H.M.F. Freundlich, Z. Phys. Chem. 57 (1906) 385.
[33] M.I. Temkin, V. Pyzhev, Acta Physiochim. URSS 12 (1940) 327.
[34] W.D. Harkins, E.J. Jura, J. Chem. Phys. 12 (1944) 112.
[35] A.M.M. Vargas, A.L. Cazetta, M.H. Kunita, T.L. Silva, V.C. Almeida, Chem. Eng. J. 168 (2011) 722.
[36] B.S. Inbaraj, J.S. Wang, J.F. Lu, F.Y. Siao, B.H. Chen, Bioresour. Technol. 100 (2009) 200.
[37] P.V. Messina, P.C. Schulz, J. Colloid Interface Sci. 299 (2006) 305.
[38] S. Karaca, A. Gürses, R. Bayrak, Energy Convers. Manage. 46 (2005) 33.
[39] S. Lagergren, Kungliga Svenska Vetenskapsakademiens, Handlingar 24 (1898) 1.
[40] Y.S. Ho, G. McKay, Process. Biochem. 34 (1999) 451.
[41] W.J. Weber Jr., J.C. Morris, J. Sanit, J. Sanit. Eng. Div., Am. Soc. Civ. Eng. 89 (1963) 31.
[42] S. Eftekhari, A. Habibi-Yangjeh, Sh. Sohrabnezhad, J. Hazard. Mater. 178 (2010) 349.
[43] K.G. Bhattacharyya, A. Sharma, Dyes Pigm. 65 (2005) 51.
[44] A.Z.A. Mahani, A.A. Jalil, S. Triwahyono, S.H. Adam, N.H.N. Kamarudin, Biochem. Eng. J. 54 (2011) 124.
[45] M.H. Kalavathy, T. Karthikeyan, S. Rajgopal, L.R. Miranda, J. Colloid Interface Sci. 292 (2005) 354.
[46] M.A. Zanjanchi, H. Golmojdeh, M. Arvand, J. Hazard. Mater. 169 (2009) 233.
[47] Y. Dong, B. Lu, S. Zang, J. Zhao, X. Wang, Q. Cai, J. Chem. Technol. Biotechnol. 86 (2010) 616.